AFRL-AFOSR-VA-TR-2024-0147

Archiving and Enhancing the DMSP Special Sensor Data

Rezy Pradipta
BOSTON COLLEGE CHESTNUT HILL MA
140 COMMONWEALTH AVE
CHESTNUT HILL, MA, 02467-3853
US

02/08/2024
Final Technical Report

Air Force Research Laboratory
Air Force Office of Scientific Research
Arlington, Virginia 22203
Air Force Materiel Command

REPORT DOCUMENTATION PAGE

PLEASE DO NOT RETURN YOUR FORM TO THE ABOVE ORGANIZATION.

1. REPORT DATE	2. REPORT TYPE	3. DATES COVERED	
20240208	Final	START DATE 20200901	END DATE 20230831

4. TITLE AND SUBTITLE
Archiving and Enhancing the DMSP Special Sensor Data

5a. CONTRACT NUMBER	5b. GRANT NUMBER	5c. PROGRAM ELEMENT NUMBER
	FA9550-20-1-0313	61102F
5d. PROJECT NUMBER	**5e. TASK NUMBER**	**5f. WORK UNIT NUMBER**

6. AUTHOR(S)
Rezy Pradipta

7. PERFORMING ORGANIZATION NAME(S) AND ADDRESS(ES)
BOSTON COLLEGE CHESTNUT HILL MA
140 COMMONWEALTH AVE
CHESTNUT HILL, MA 02467-3853
US

8. PERFORMING ORGANIZATION REPORT NUMBER

9. SPONSORING/MONITORING AGENCY NAME(S) AND ADDRESS(ES)	10. SPONSOR/MONITOR'S ACRONYM(S)	11. SPONSOR/MONITOR'S REPORT NUMBER(S)
Air Force Office of Scientific Research 875 N. Randolph St. Room 3112 Arlington, VA 22203	AFRL/AFOSR RTB1	AFRL-AFOSR-VA-TR-2024-0147

12. DISTRIBUTION/AVAILABILITY STATEMENT
A Distribution Unlimited: PB Public Release

13. SUPPLEMENTARY NOTES

14. ABSTRACT
After more than five decades of continuous observations, the Defense Meteorological Satellite Program (DMSP) has perhaps the richest legacy of any space-based earth observing system. Since the introduction of space environment sensors in 1976 it has served as a staple data source for the heliophysical community. Currently, three satellites (DMSP F16, F17, and F18) remain in service and the data are more relevant than ever before, augmented by results from other missions and numerous ground-based sensors. In this work, we perform a continual archiving of the DMSP observation data from the special sensor suite (SSIES, SSJ5, and SSM) on the distributed Madrigal system, allowing the processed DMSP data to reach a wider scientific user community. In addition, we are also working towards providing additional, value-added tools and products based on the DMSP special sensor suite data. Further, we utilize the available time and the DMSP observation data for a number of scientific investigations in order to advance DMSP's role in understanding our geospace environment. These investigations include an event analysis of the Port Beirut explosion that occurred on 4 August 2020, an analysis of ionospheric response to the annular solar eclipse on 26 December 2019 over Southeast Asia, an analysis of disturbances originating from the 15 January 2022 Tonga volcano eruption, a numerical study of Shannon information content as a quantitative global measure of perturbed ionospheric state, and an investigation of increased ionospheric fluctuations during the summer 2021 North American heat wave event. The multi-instrument analysis of the 4 August 2020 Beirut explosion and the 15 January 2022 Tonga eruption demonstrate the use of DMSP observation in combination with ground-based ionosondes as a powerful combination. The apparent increase in the level of ionospheric fluctuations during the 2021 heat wave event may have implications on possible ways for climate change and global warming to impact ionosperic space weather.

15. SUBJECT TERMS

16. SECURITY CLASSIFICATION OF:			17. LIMITATION OF ABSTRACT	18. NUMBER OF PAGES
a. REPORT U	b. ABSTRACT U	c. THIS PAGE U	UU	18

19a. NAME OF RESPONSIBLE PERSON	19b. PHONE NUMBER *(Include area code)*
JULIE MOSES	426-9586

Standard Form 298 (Rev.5/2020)
Prescribed by ANSI Std. Z39.18

Archiving and Enhancing the DMSP Special Sensor Data

Rezy Pradipta

Boston College, Institute for Scientific Research

Final Report, 29 November 2023

Abstract

After more than five decades of continuous observations, the Defense Meteorological Satellite Program (DMSP) has perhaps the richest legacy of any space-based earth observing system. Since the introduction of space environment sensors in 1976 it has served as a staple data source for the heliophysical community. Currently, three satellites (DMSP F16, F17, and F18) remain in service and the data are more relevant than ever before, augmented by results from other missions and numerous ground-based sensors. In this work, we perform a continual archiving of the DMSP observation data from the special sensor suite (SSIES, SSJ5, and SSM) on the distributed Madrigal system, allowing the processed DMSP data to reach a wider scientific user community. In addition, we are also working towards providing additional, value-added tools and products based on the DMSP special sensor suite data. Further, we utilize the available time and the DMSP observation data for a number of scientific investigations in order to advance DMSP's role in understanding our geospace environment. These investigations include an event analysis of the Port Beirut explosion that occurred on 4 August 2020, an analysis of ionospheric response to the annular solar eclipse on 26 December 2019 over Southeast Asia, an analysis of disturbances originating from the 15 January 2022 Tonga volcano eruption, a numerical study of Shannon information content as a quantitative global measure of perturbed ionospheric state, and an investigation of increased ionospheric fluctuations during the summer 2021 North American heat wave event. The multi-instrument analysis of the 4 August 2020 Beirut explosion and the 15 January 2022 Tonga eruption demonstrate the use of DMSP observation in combination with ground-based ionosondes as a powerful combination. The apparent increase in the level of ionospheric fluctuations during the 2021 heat wave event may have implications on possible ways for climate change and global warming to impact ionosperic space weather.

I. Accomplishments

We performed routine processing and archiving of the Defense Meteorological Satellite Program (DMSP) observation data from the special sensor suite (SSIES, SSJ5, and SSM) on several data platforms. These data platforms include the Boston College DMSP summary webpage, NOAA archive, and the distributed Madrigal database system, allowing the processed DMSP data to reach wider scientific user community. At present, three satellites (DMSP F16, F17, and F18) are in service to provide the observation data. The processed data types generated include ion number density (and light/heavy ion fractions), horizontal and vertical components of ion drift velocity, magnetic field, ion and electron plasma temperature, spacecraft electric potential, ion and electron number density fluxes, as well as ion and electron energy fluxes.

Beyond the routine DMSP data processing and archiving, we utilized the available time and the observation data for scientific investigations, in order to expand the role of DMSP data suite in understanding the geospace environment and threats from various space weather events. Here, we describe on our DMSP-based investigation of the Port Beirut explosion on 4 August 2020 by comparison to propagation curves extracted from data graphs found in other published works. We also report findings from our analysis of multi-instrument (DMSP, ionosonde, and GNSS TEC) observation data following the 15 January 2022 Hunga Tonga volcano eruption event, and an annular solar eclipse event on 26 December 2019 over Southeast Asia. Further, we report a numerical study exploring the use of Shannon information content (SIC) as a potentially useful quantitative global measure of perturbed ionospheric TEC configuration. Finally, we report the identification, using DMSP observation data, of some ionospheric density fluctuations over areas affected by the summer 2021 heat wave event over the North American region.

Several publications/articles that have resulted from this AFOSR support:

Pradipta, R., B. A. Carter, J. L. Currie, S. Choy, P. Wilkinson, P. Maher, and R. Marshall (2023), On the propagation of traveling ionospheric disturbances from the Hunga Tonga-Hunga Ha'apai volcano eruption and their possible connection with tsunami waves, *Geophysical Research Letters*, 50, e2022GL101925, https://doi.org/10.1029/2022GL101925.

Harjosuwito, J., A. Husin, V. Dear, J. Muhamad, A. Faturahman, A. Bahar, Erlansyah, A. Syetiawan, and R. Pradipta (2023), Ionosonde and GPS total electron content observations during the 26 December 2019 annular solar eclipse over Indonesia, *Ann. Geophys.*, 41, 147–172, https://doi.org/10.5194/angeo-41-147-2023.

Carter, B. A., R. Pradipta, T. Dao, J. L. Currie, S., Choy, P. Wilkinson, et al. (2023), The ionospheric effects of the 2022 Hunga Tonga Volcano eruption and the associated impacts on GPS Precise Point Positioning across the Australian region, *Space Weather*, 21, e2023SW003476, https://doi.org/10.1029/2023SW003476.

Pradipta, R. and Lai, P.-C. (2023), Observations of Ionospheric Disturbances Associated with the 4 August 2020 Port Beirut Explosion by DMSP and Ionosondes, manuscript submitted to *Ann. Geophys.* (under review), https://doi.org/10.5194/angeo-2023-36.

Pradipta, R., and Kim, B. (2023), Characterizing perturbed ionospheric total electron content configurations using the Shannon information content, manuscript submitted to *Adv. Space Res.* (under review).

Routine DMSP Data Processing and Archiving

The raw DMSP observation data are processed at Boston College. Afterward, the processed data are sent via network drop boxes to the MIT Madrigal database (http://cedar.openmadrigal.org/) and to the National Oceanic and Atmospheric Administration (NOAA) for long-term archiving. This means of data distribution facilitates their access by the wider scientific community. In addition, summary plots of the DMSP observations (for both low-latitude and high-latitude

regions) are also provided on the Boston College DMSP webpage (https://dmsp.bc.edu) for a general convenience in quick-look viewing.

The processing of DMSP data can be schematically summarized in Figure 1. The program exday.com reads the raw files to check and order the data into binary 24-hour files. The 24-hour files are inputs for the Ground Processing Software (GPS), which are also sent to Madrigal and NOAA for their DMSP database. The GPS program generates Environmental Data Record (EDR) data from the SSIES and Magnetic Field Record (MFR) data from the SSM. The EDR and MFR files are also saved in the DMSP Dropbox provided for MIT Madrigal. The MIT Madrigal database reformats these files into Madrigal-compatible files. The Table shown at the bottom of Figure 1 illustrates some examples of filename in each step. The characters printed in bold are variables. Specifically, **n** is sensor number; **NN** marks the spacecraft number; **YY** is year; **ddd** is day-of-year; **YYYYMMDD** is 4 digit year, 2 digit month, and 2 digit day; **HHMMSS** = 2 digit hour, 2 digit minute, and 2 digit second for start time of file; **hhmmss** = 2 digit hour, 2 digit minute, and 2 digit second for end time of file.

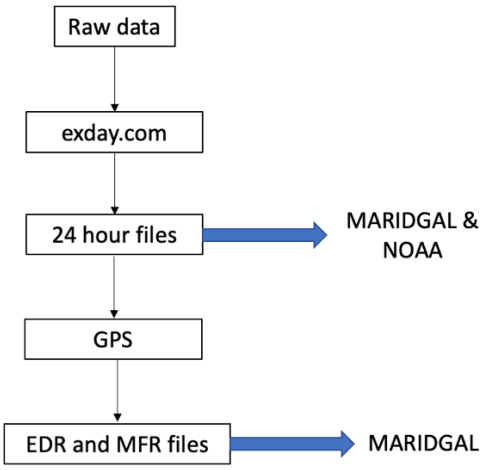

File	Filename example
Raw data	f18_57959_20210122305_i3_00.dat - SSIES f18_57959_20210122305_j5_00.dat - SSJ f18_57959_20210122305_mm_00.dat – SSM
Input of job file	r20210830743.i17; r20211082227.j17; r20211272056.m15
output of job file/Input of GPS	iesf**NNYYddd** ; ephf**NNYYddd** ; ssmf**NNYYddd**
Output of GPS	PS.CKGWC_SC.U_DI.A_GP.SIES**n**-F**NN**-R99990-B9999090-APGA_AR.GLOBAL_DD.**YYYYMMDD**_TP.**HHMMSS**-**hhmmss**_DF.EDR PS.CKGWC_SC.U_DI.A_GP.SSMXX-F**NN**-R99990-B9999090-APSM_AR.GLOBAL_DD.**YYYYMMDD**_TP.**HHMMSS**-**hhmmss**_DF.MFR

Figure 1. Schematic flowchart of the DMSP data processing and the filename convention.

Analysis of Ionospheric Response to the 4 Aug 2020 Beirut Explosion

On 4 August 2020 at approximately 15:08 UTC, a large explosion occurred at the Port of Beirut, Lebanon (33.9°N 35.52°E). The explosion appeared to have been caused by roughly 2750 tons of ammonium nitrate that had caught fire in a storage building [*Guglielmi*, 2020]. Some early reporting mentioned that the shockwave from the explosion was heard 200 km away in Cyprus.

Such a massive explosion may produce wave disturbances that reach the upper atmosphere and the ionosphere. Roughly an hour after the moment of explosion, the DMSP satellite F17 was at its ascending orbit at longitude 35°E, which was nearby Beirut's longitude sector. We decided to investigate any signatures of traveling ionospheric disturbances (TIDs) induced by acoustic-gravity waves (AGWs) from the Beirut explosion, which the DMSP satellite might be able to intercept given the serendipitous timing of the satellite pass and the magnetic latitude.

The geomagnetic condition on 4 August 2020 was relatively quiet with no geomagnetic storm event (min Dst = -14 nT and max Kp = 3^{+}), which effectively ruled out auroral LSTIDs that may be intruding into the midlatitude regions from high-latitudes.

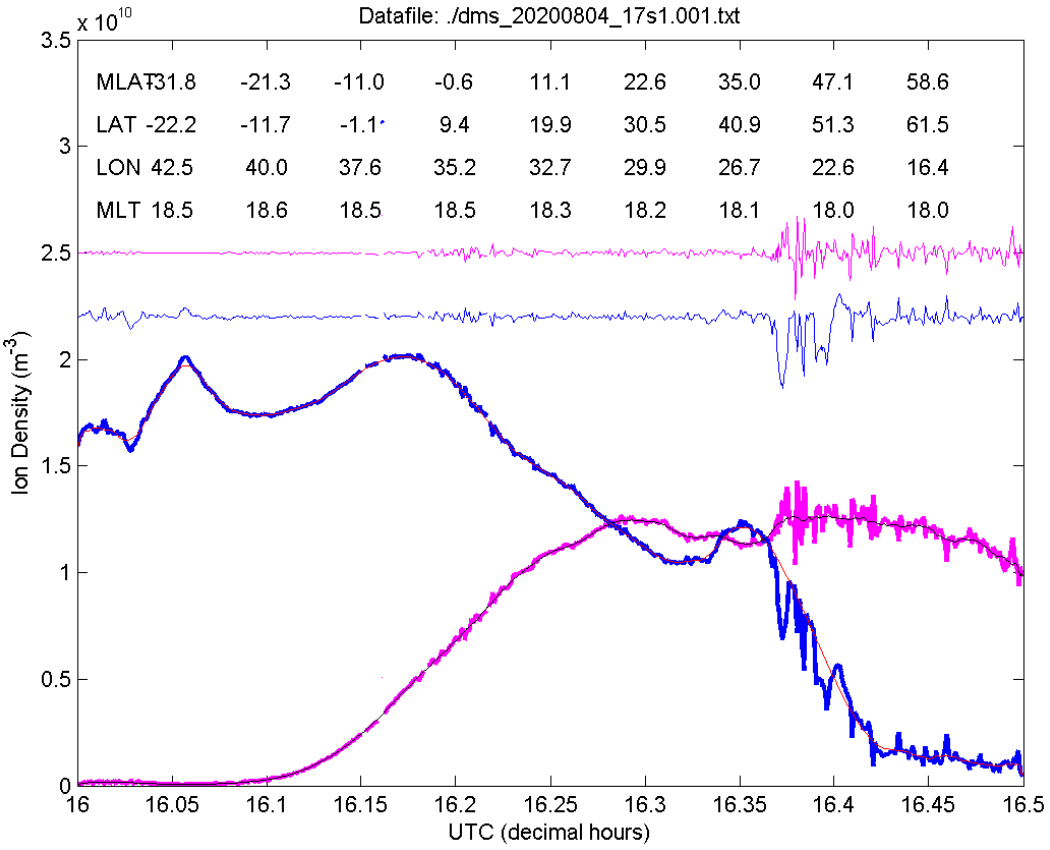

Figure 2. Heavy (O+) and light (H+, He+) ion density data observed during DMSP F17 satellite pass near Beirut's longitude sector on 4 August 2020. Both original and detrended ion density values are shown. The O+ densities are shown in magenta, and light ion densities (H+, He+) are shown in blue.

In the data analysis, we used the low-latitude section of ion density observations from DMSP F17 spacecraft recorded on 4 August 2020, and focused our attention on an ascending orbit pass starting at around 16:12 UTC over longitude sector 35°E (which corresponds to 18.5 MLT at the start of this ascending orbit pass). The ion density data were detrended using a polynomial fit to construct a smooth baseline, and the net ion density fluctuations (i.e. original ion density data minus the smooth baseline) should reveal any signatures of AGW/TID that the DMSP F17 was able to intercept at its orbit (~850 km altitude above sea level).

Figure 2 shows the observed fluctuations in the DMSP F17 ion density data, represented as a time series plot during the aforementioned ascending orbit pass. We have separated the DMSP ion density data into O^+ ions and light ions (H^+, He^+). The heavy (O^+) ion density is shown as a bold magenta curve (with the smooth baseline from polynomial fit shown as a thin black curve). The density of light ions (H^+, He^+) is shown as a bold blue curve (with the smooth baseline from polynomial fit shown as a thin red curve). The detrended heavy (O^+) and light (H^+, He^+) ion densities are shown as light magenta and blue curves, respectively. Note that the detrended ion density time series are displayed with vertical offsets. A number of additional orbit parameters (MLAT, LAT, LON, and MLT) are also shown as text on the upper rows of the graph.

In the time series plot, it is quite clear that there were some fluctuations between UTC = 16.35 hr and UTC = 16.45 hr (even before detrending). These fluctuations were quite strong, and they might be associated with the Beirut explosion. Comparison with a set of control data recorded in July 2020 (on 4, 5, 12, 20, 27, and 28 July 2020 – which consisted of similar DMSP F17 orbits) indicates that the abovementioned ion density fluctuations were indeed anomalous and quite unique to 4 August 2020.

Further, cross-examinations of the DMSP F17 satellite observations against ionograms that were recorded on 4 August 2020 by several digisonde stations in the Mediterranean area also support the scenario that there were some anomalous fluctuations associated with the Beirut explosion. Ionograms from Nicosia (35.03°N 33.16°E – 250 km from Port Beirut), Athens (38°N 23.5°E – 1172 km from Port Beirut), and San Vito (40.6°N 17.8°E – 1731 km from Port Beirut) were included in the cross-examination. These ionograms were retrieved from the University of Massachusetts Lowell's Digital Ionogram Database (DIDBase).

Figure 3 shows a geographic map delineating the spatial configuration of the digisonde stations relative to Beirut (where the explosion had happened) and the point coordinates of AGW/TID interceptions by the DMSP F17 satellite on 4 August 2020. In addition, Figure 3 also shows a set of sample ionograms from the Nicosia station, in which TID signatures were apparent in the form of a loop and *z*-shaped twists in the ionogram trace. Examination of additional ionograms from the same locations on a few days leading to 4 August 2020 did not show such patterns, indicating that the distinct AGW/TID signatures observed on 4 August 2020 were probably associated with a unique event on that day (viz. the Beirut explosion). These additional checks with regard to the local background pattern of AGW/TID is necessary since the Beirut explosion event had happened near dusk sector, during which the dusk terminator may also produce some recurring diurnal AGW/TID. The checks we performed indicate that the disturbances originating from the ammonium nitrate explosion at Beirut was either stronger or exhibiting more distinct signatures in comparison to diurnally recurring AGW/TID.

Among the 3 (three) digisonde stations under examination, we note that AGW/TID signatures detected at San Vito station were not as clear/distinct as the AGW.TID signatures detected at Nicosia and Athens stations. At San Vito station, the AGW/TID signatures were mainly seen as forking/branching of the ionogram traces and slight frequency spread echoes (no formation of loops or z-shaped twists such as those observed at Nicosia and Athens).

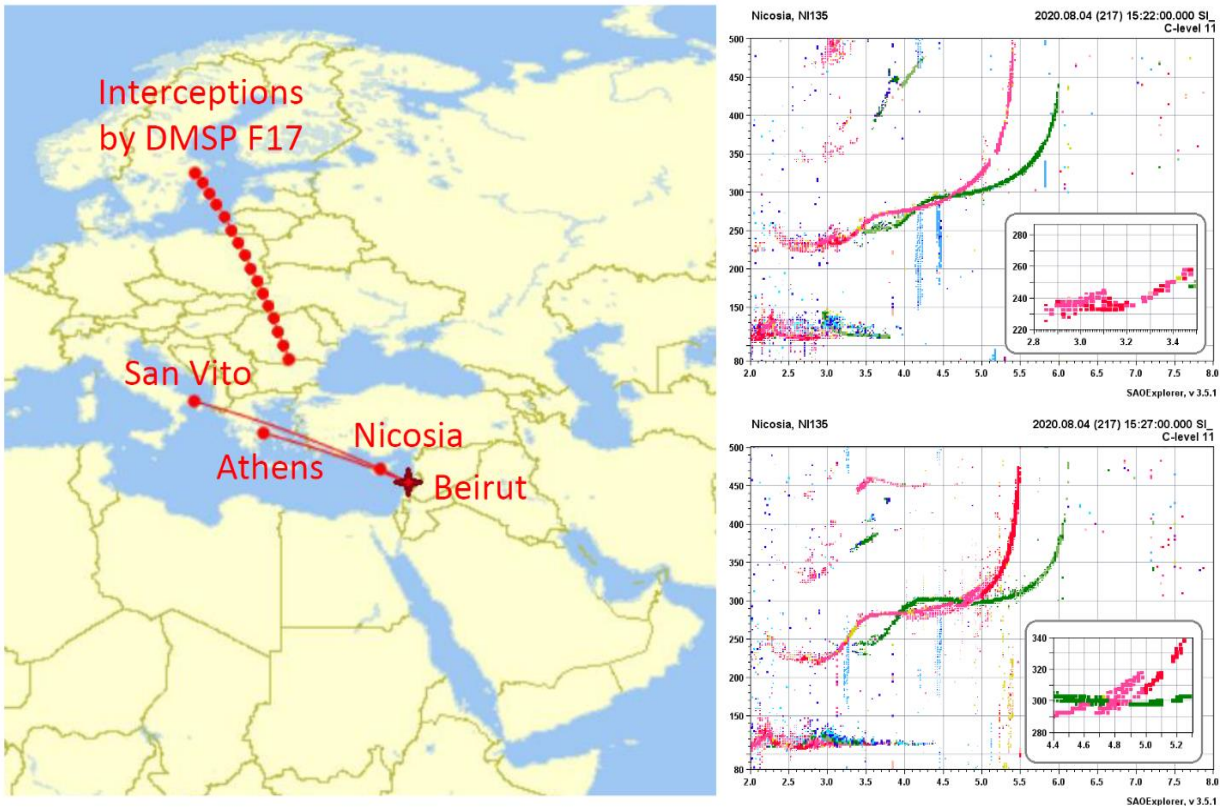

Figure 3. Left panel: situational map of the area around Beirut (explosion site) showing the coordinate locations of AGW/TID interception by the DMSP F17 satellite and the nearby ground-based digisonde stations. Right panels: representative samples of recorded ionograms from the Nicosia station shortly after the Beirut explosion on 4 August 2020.

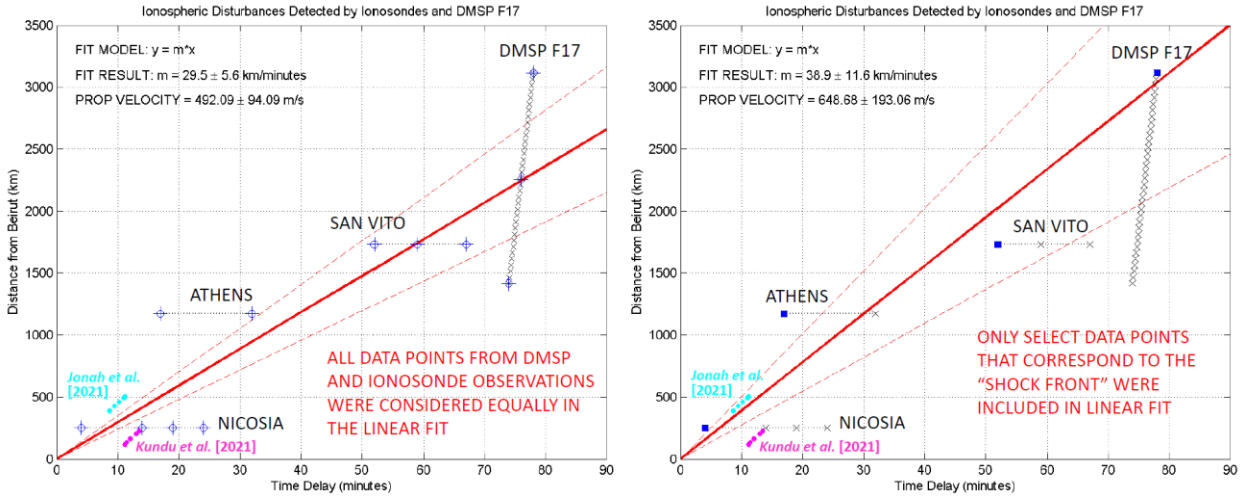

Figure 4. Kinematics analysis of the propagation of AGW/TID suspected to have originated from Beirut explosion on 4 August 2020. Two types of kinematics calculations were performed. Left panel: analysis using all DMSP + digisonde data points equally in the linear fit (estimated TID velocity = 492 m/s). Right panel: analysis using only select data points for the linear fit (estimated TID velocity = 649 m/s). Cyan and magenta circles are data points extracted from graphs published in Kundu et al. [2021] and Jonah et al. [2021], who also investigated the TIDs from this event.

Figure 4 shows the kinematics analysis for estimating the propagation speed of the observed AGW/TID, which were suspected to have originated from the Beirut explosion. Two types of the wave kinematics calculations were performed. One version uses all the data points equally in the linear fit (left panel in Figure 4), while the other version only fits a select group of data points that corresponded to the "shock front" that traveled ahead of the rest of the wave disturbances (right panel in Figure 4). The former yields TID velocity of 492.1 ± 94.1 m/s. Meanwhile, the latter yields 648.7 ± 193.1 m/s as the estimated TID velocity. Considering the uncertainty in the linear fit parameters, there is some overlap between the two estimates. However, there are valid reasons to suspect that the difference between the two might actually be systematic (i.e. wave disturbances in the form of "shock front" can be expected to travel faster than regular wave fluctuations).

There are two other studies on the TIDs suspected to have originated from the Beirut explosion [*Kundu et al.*, 2021; *Jonah et al.* 2021]. Both of these studies had used TEC data in the vicinity of Beirut area, up to a distance of approximately 500 km. *Kundu et al.*'s [2021] analysis of the event yielded a TID propagation velocity of approximately 800 m/s. Meanwhile, *Jonah et al.*'s [2021] analysis yielded a TID propagation velocity of approximately 750 m/s. Based on the data graphs and tables from these two published works, we extracted the data points associated with the progression of AGW/TID from Beirut and added them to the wave kinematics analysis plot (cf. Figure 4). The data points from *Kundu et al.* [2021] are shown in Magenta, and those from *Jonah et al.* [2021] are shown in cyan. Comparison against these published data points shows that the first type of kinematics analysis produces a propagation curve that falls almost exactly in between *Kundu et al.*'s [2021] and *Jonah et al.*'s [2021] results. The same comparison shows that the second type of kinematics analysis produces a propagation curve that more closely agrees with *Jonah et al.*'s [2021] result, and a greater discrepancy from *Kundu et al.*'s [2021] result. However, we must also remember that our combined DMSP + digisonde data analysis involved propagation distances of up to 3000 km, which is much longer than the range covered by either *Kundu et al.*'s [2021] and *Jonah et al.*'s [2021]. There may be some fundamental differences between near-field and far-field behavior of the wave disturbances, including the possibility of the shock wave propagating with a fast initial propagation and subsequently decelerated after going past the near-field regime. As another point of comparison, in the lower atmosphere, a significantly slower wave propagation speed of around 344 m/s, closer to the acoustic speed, was reported by *Pilger et al.* [2021] based on the Comprehensive Nuclear-Test-Ban Treaty (CTBT) sensors.

Analysis of Ionospheric Disturbances from the 15 Jan 2022 Tonga Eruption

On 15 January 2022 at approximately 04:15 UTC, the Hunga Tonga-Hunga Ha`apai volcano erupted after several days of increased geological activity [*United States Geological Survey*, 2022; *Nidumolu et al.*, 2022; *Fountain*, 2022; *Francis et al.*, 2022]. The eruption registered as Magnitude 5.8 in earthquake records, and the plumes from the eruption reached 58 km in altitude [*United States Geological Survey*, 2022; *Yuen et al.*, 2022]. Tsunami waves were also produced by the massive eruption [*Kubota et al.*, 2022; *Gusman and Roger*, 2022]. Further, raw optical imageries from earth-observing satellites captured the blast waves that emanated from the eruption site [*Duncombe*, 2022; *Sidder*, 2022]. Based on the magnitude of the eruption, it was suspected from the outset that some significant ionospheric effects would be manifested on a

global scale as well. We decided to examine whether DMSP observations had intercepted wave fluctuations associated with the eruption. In our analysis of the DMSP F17 observation data, we found strong wave fluctuations in the general vicinity of Japan, confirmed by ground-based observations using regional ionosondes operated by the National Institute of Information and Communications Technology (NICT).

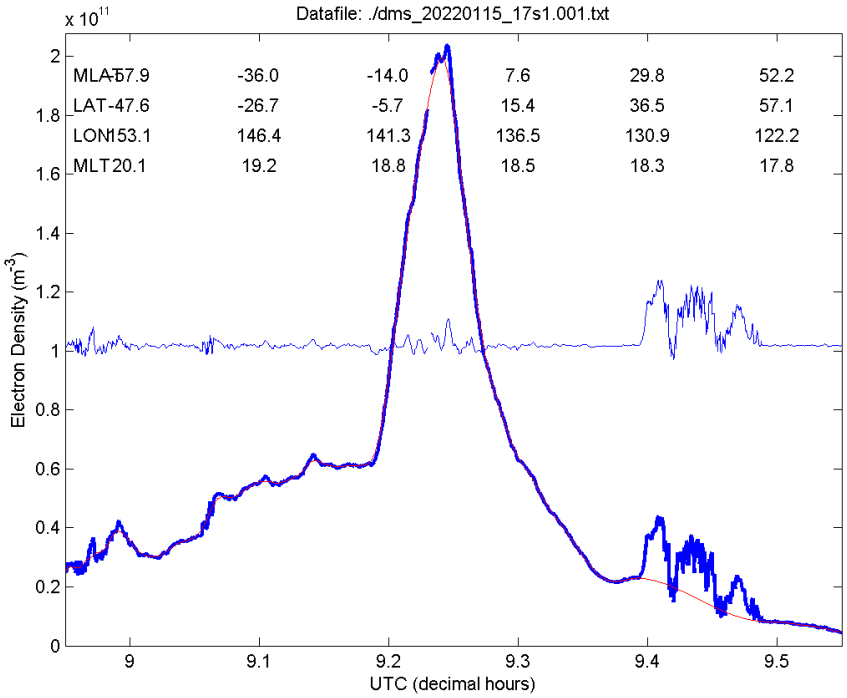

Figure 5. Ion density data observed during DMSP F17 satellite pass near Japan's longitude sector on 15 January 2022. Both original and detrended ion density values are shown. Anomalous fluctuations in ion density were observed near 9:30 UTC between geographic latitude 36.5° and 57.1°N (between magnetic latitude 29.8° and 52.2°).

Figure 5 shows a time series plot of ion density measurements from DMSP F17 spacecraft near Japan's longitude sector on 15 January 2022. The ion density observations were detrended using polynomial fit in order to highlight wave fluctuations that are present in the data. The original ion density data are shown as a bold blue curve, and the detrended ion density data are shown as a lighter blue curve. Strong fluctuations can be seen between *UTC* = 9.4 hr and *UTC* = 9.5 hr (before and after detrending). Specifically after detrending, a set of smaller wave fluctuations are visible between *UTC* = 9.2 hr and *UTC* = 9.3 hr. The former is of primary interest to us, due to the relatively large intensity of the fluctuations. Figure 6 shows the geospatial representation of these strong fluctuations, which occur just to the northwest of Japan. The location of Tonga eruption is marked on the map (with a star on the left panel, and with blue circles on the right panel). A set of cyan curves are also drawn on the right panel in Figure 6, indicating the expected locations of the wavefronts (assuming 300 m/s propagation velocity) at +7, +8, and +9 hours after the Tonga eruption. Green circles on the right panel in Figure 6 indicate the locations of several regional ionosonde stations operated by the NICT. From north to south, these are Wakkanai, Kokubunji, Yamagawa, and Okinawa stations, respectively.

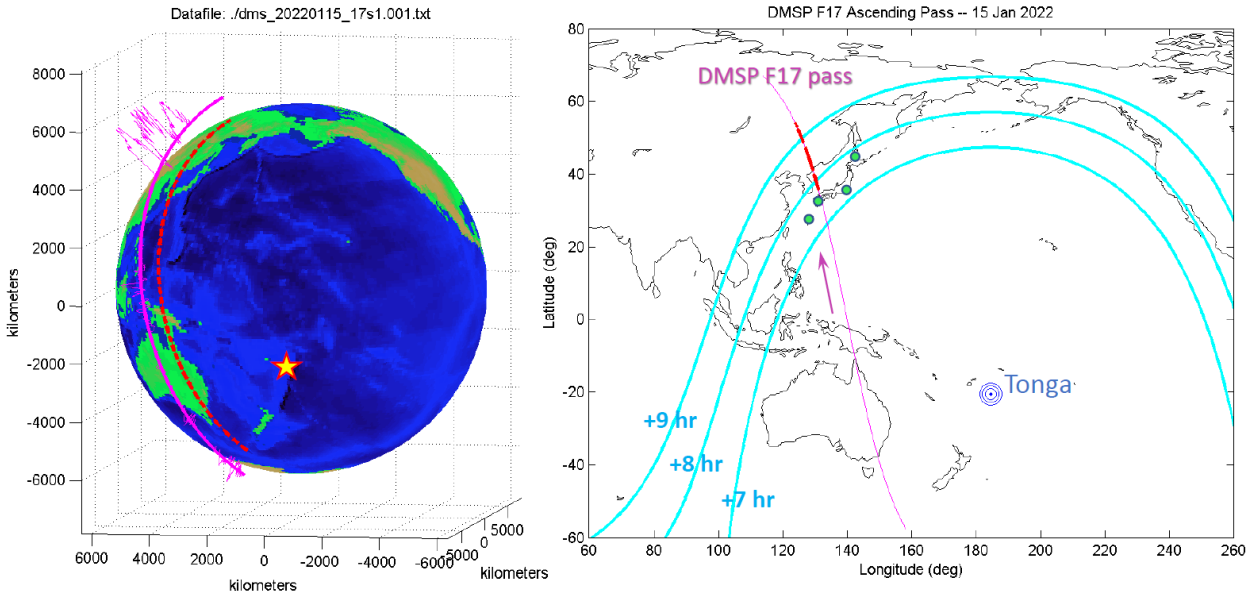

Figure 6. Geospatial representation of the ion density fluctuations that were intercepted by DMSP F17 on 15 January 2022 near Japan's longitude sector. NICT's ionosondes are marked with green circles.

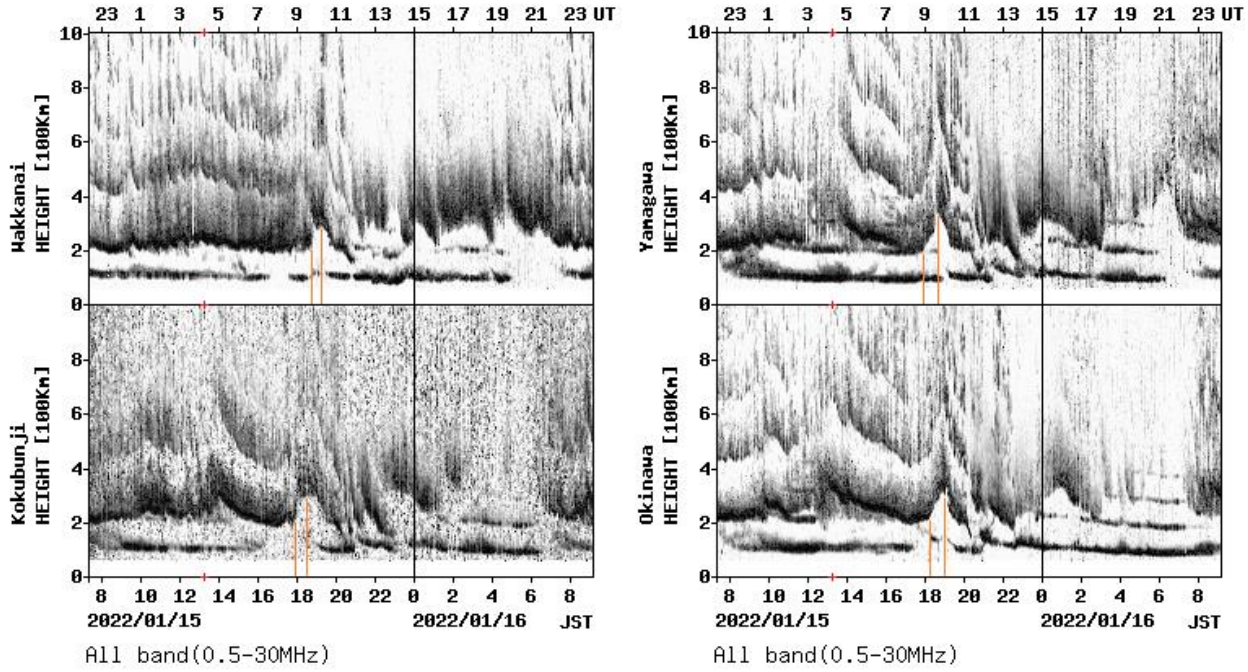

Figure 7. Summary plots of observations by the NICT ionosondes on 15 January 2022. Vertical orange lines indicate the estimated epochs when an anomalous uplift occurred over each ionosonde station.

Figure 7 shows a set of range-time-intensity (RTI) summary plots of the ionosonde observations at the 4 (four) aforementioned locations in Japan on 15 January 2022. An anomalous uplift of the F-region ionosphere was observed over each ionosonde station at approximately 09:00 UTC. This large uplift of ionospheric layer was not observed in the preceding days, indicating that is unique to 15 January 2022 and likely related to the Tonga eruption. The precise timing is also consistent with what was observed in the DMSP F17 data. The NICT ionosondes are closer to

Tonga than the location of wave fluctuations intercepted by DMSP (cf. Figure 6). Thus, if the disturbances had originated from the Tonga eruption, it is logical that they are detected first by the NICT ionosondes (at approximately *UTC* = 9 hr) and sometime later to the northwest of Japan by the DMSP F17 spacecraft (at approximately *UTC* = 9.5 hr).

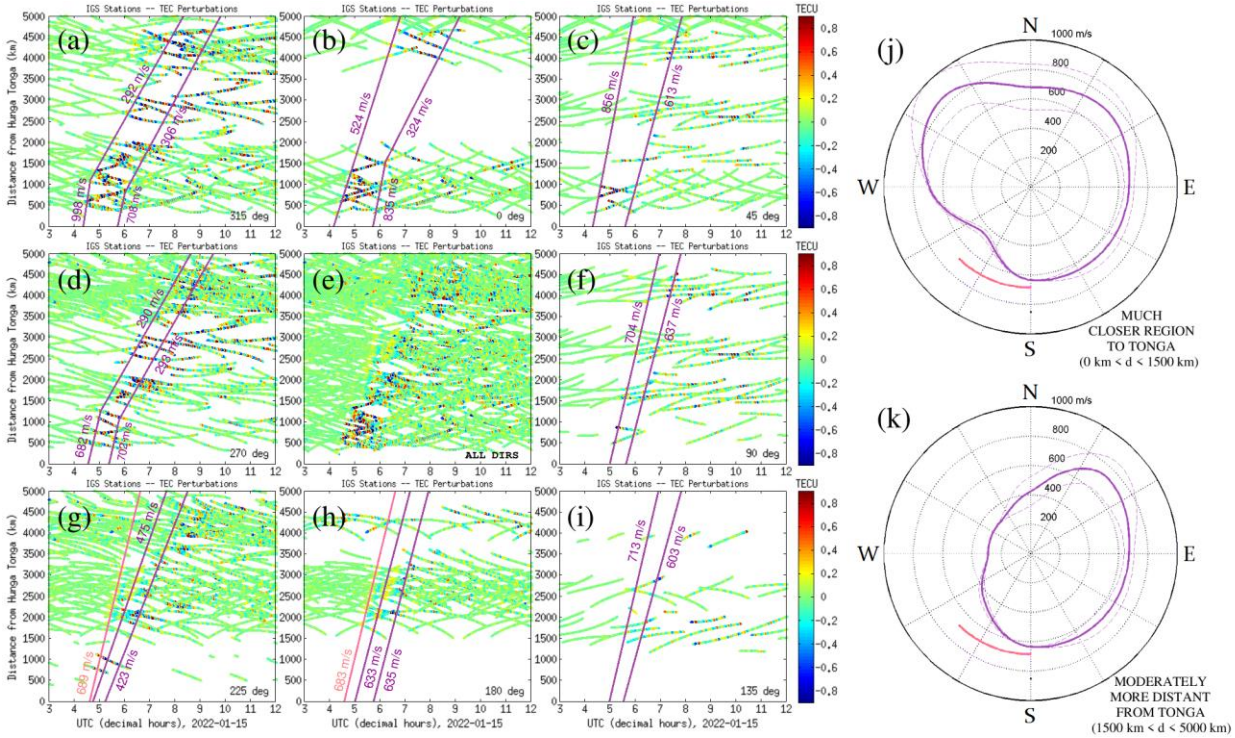

Figure 8. (a-i) Colormap plots of TECP values as a function of distance from Tonga and UTC on 15 January 2022 (magnified around 03:00–12:00 UTC and 0–5,000 km), divided into ±45° wedges around the eight cardinal and intercardinal directions. (j, k) Polar plots of estimated TID velocities as a function of bearing angle in the near-field and mid-distance-field.

In addition, we also analyzed GPS TEC data in the vicinity of the Tonga volcano to determine the azimuthal profile of the propagation velocity of the ionospheric disturbances. From the calibrated TEC data, we derived the TEC perturbations (TECP) values and plotted these values in space-time graphs for different wedges corresponding to various directions. The analysis would reveal whether there was some anisotropy in the propagation velocity of ionospheric disturbances with respect to the azimuth angle.

Figure 8 shows the result of this analysis. The left hand side of the figure displays the space-time plots for various azimuthal propagation angle. The general progression of the disturbances is marked (bounded) by the auxiliary lines. The right hand side shows the azimuthal profiles of the propagation velocity. The azimuthal profiles show a significant asymmetry, which changes with distance from near-field to mid-distance-field. Subsequent comparison against the shape of the tsunami wavefront on the ocean around Tonga reveal the same kind of bean-shaped velocity profile. This pattern indicates that in the near-field and mid-distance-field, the progression of the ionospheric disturbances was still strongly controlled by the shape of the tsunami wavefront on the ocean surface.

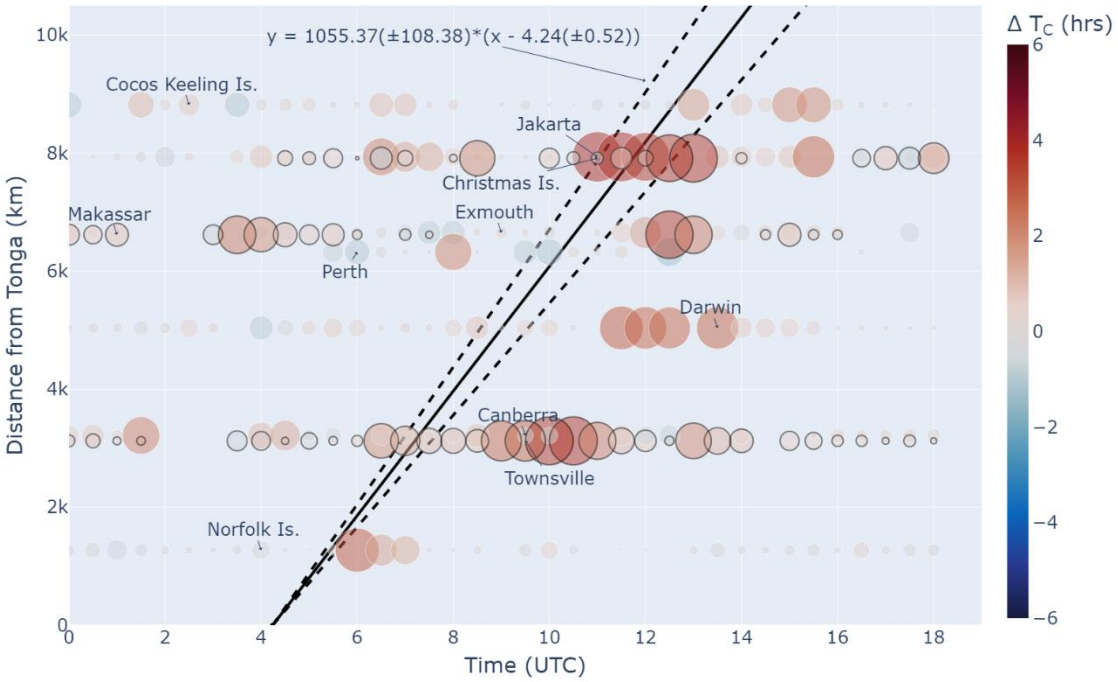

Figure 9. Distance from Tonga versus time colored/marked according to the change in GPS Precise Point Positioning (PPP) convergence time. Greater circles mean longer convergence time. Black lines indicate the propagation line of TIDs from the Tonga volcano eruption.

In terms of possible effects the Tonga eruption might have on modern space-based technology, we investigated the performance of GPS precise point positioning (PPP) over Australia during the relevant time period. We found that the accuracy of GPS PPP was generally not affected by the ionospheric disturbances from the Tonga volcano eruption. However, the convergence time required for GPS PPP applications was found to increase significantly. In other words, under this severely disturbed ionospheric condition, it took longer for GPS PPP to achieve a reliable lock on the true coordinate. This effect is shown in Figure 9. In places located near the wavefront of ionospheric disturbances generated by the Tonga eruption, the GPS PPP convergence time was found to increase, up to ~5 hours.

Ionospheric Response to the 26 Dec 2019 Annular Solar Eclipse Event

An annular solar eclipse occurred over Southeast Asia on 26 December 2019. This was a unique event since the eclipse trajectory passed over the locations of the equatorial ionization anomaly (EIA) in low-latitude region. We investigated the ionospheric response to this solar eclipse event to determine if there are any interesting features. Figure 10 shows the solar eclipse trajectory, and several cross-sectional cut lines that we drew for a close examination of the TEC variation. For this solar eclipse investigation, we worked with a number of space scientists from LAPAN (the Indonesian space research agency) to obtain the ground measurements.

The GPS TEC data were obtained from a number of receiver stations in Sumatra. These stations are part of a larger CORS network for geodetic applications. Using the calibrated TEC data, we

determined the quiet baseline and calculated the net change in TEC (=ΔTEC values) by subtracting the aforementioned baseline.

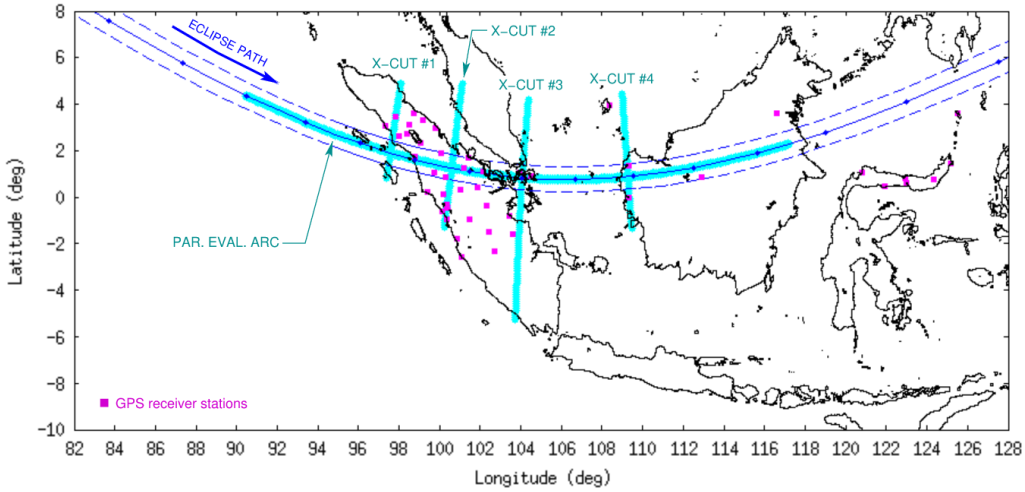

Figure 10. Trajectory of the 26 December 2019 annular solar eclipse, and several cross-sectional cut lines for evaluating dynamical changes in TEC as a response to the eclipse.

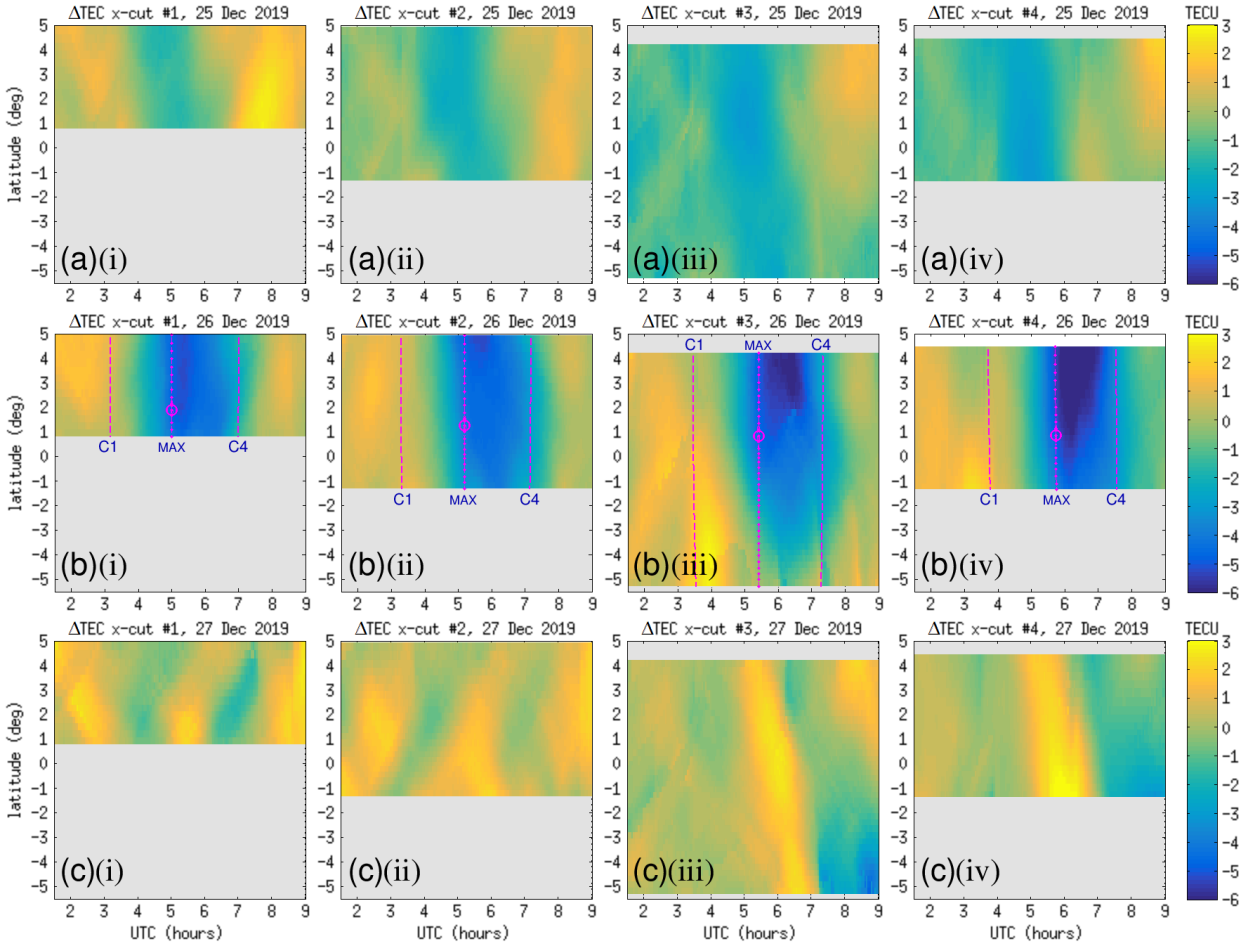

Figure 11. Plot of ΔTEC as a function of UTC and latitude (along the various cut lines) before, on, and after the day of the solar eclipse.

Figure 11 shows a set of ΔTEC plots on 25-27 December 2019 for the various cut lines depicted in Figure 10. Top row is for 25 December 2019 (the day before eclipse), the middle row is for 26 December 2019 (the eclipse day), and the bottom row is for 27 December 2019 (the day after the eclipse). Dashed lines mark the phases of the eclipse (from initial contact C1, to maximum eclipse, until the final contact C4). The circle marks the center of the eclipse (i.e. annularity). Darker blue color indicates deeper TEC depletions. An interesting feature was found here, that the deepest TEC depletions actually occurred to the north of the central annularity, even though the lunar shadow was directed slightly from the south. This means that the darkest area from the eclipse was experiencing weaker effect in terms of ionospheric changes. From our analysis, we conclude that this peculiar pattern was caused by the equatorial fountain effect, which siphoned plasma from the geomagnetic equator (located to the north of the eclipse path in this case) and transported the charged particles to the EIA crests. This flow provided some buffer for plasma in the EIA crests to "resist" the solar eclipse effect, but it depleted much of the plasma along/near the geomagnetic equator.

Using Shannon Information as Quantitative Measure of TEC Perturbations

Traditionally, perturbed ionospheric TEC configurations are characterized using the magnitude of TEC deviation from a defined "baseline" level, or perhaps using the magnitude of tilt/gradient that are present. A new idea was explored to utilize a concept borrowed from information theory to help quantify how out-of-equilibrium the ionospheric TEC configuration is at a certain time. This particular concept is known as the Shannon Information Content (SIC).

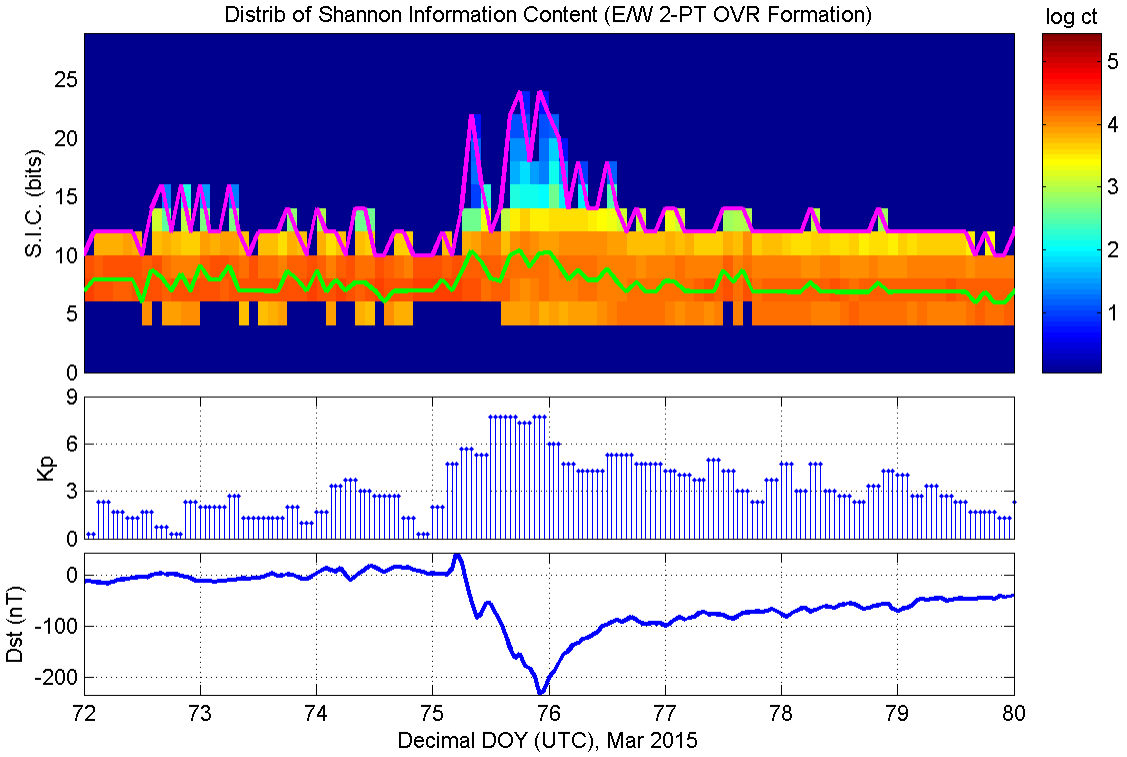

Figure 12. Plot of Shannon information content variation on 14-21 March 2015, along with Kp and Dst time series for the same time period. We observed that SIC was significantly enhanced during the period of St. Patrick's Day geomagnetic storm, which started on 17 March 2015.

The main idea behind the usage of SIC is not to focus on the magnitude of TEC deviation from its baseline, but rather to focus on the probability p for such TEC deviation to occur according to long-term climatology. Given the value of p, the numerical value for SIC itself is given by the simple expression $\log_2(1/p)$. The elegant aspect of SIC is that the rarer the configuration (i.e. the lower the probability p), the higher SIC will be; and the standard unit of SIC is in bits (i.e. the fundamental unit of information). A high SIC value can be interpreted as a highly surprising outcome that warrants a close attention, which is almost always the case for a highly perturbed ionospheric TEC configuration.

We performed some tests of this new concept, using global ionospheric map (GIM) data from the International GNSS Services (IGS) to build the underlying long-term climatology that is needed for the SIC computation. A case in point from these tests is depicted in Figure 12. The top panel shows a dynamic histogram of SIC values over the whole globe. The green and magenta curves track the mean and ceiling of SIC values globally over the time period shown. When a strong geomagnetic storm occurred (in this case the 17 March 2015 Saint Patrick's Day Storm), which corresponds to time period of elevated Kp and very negative Dst, we observed that SIC values were also enhanced. During geomagnetic storms, it is empirically known that the ionospheric TEC configuration would go out-of-equilibrium (e.g. due to positive and negative storm phases). The enhanced SIC values during storm period demonstrate the basic concept that SIC could be used in fundamental way to characterize out-of-equilibrium ionospheric TEC configuration.

Increased Ionospheric Fluctuations during Summer 2021 Heat Wave Event

A severe and prolonged heat wave event occurred over North America during summer 2021, as illustrated in Figure 13. We are interested in investigating a scenario in which thermal gradients associated with a severe heat wave event generate wave disturbances that cause the ionosphere over the affected area to exhibit greater level of fluctuations.

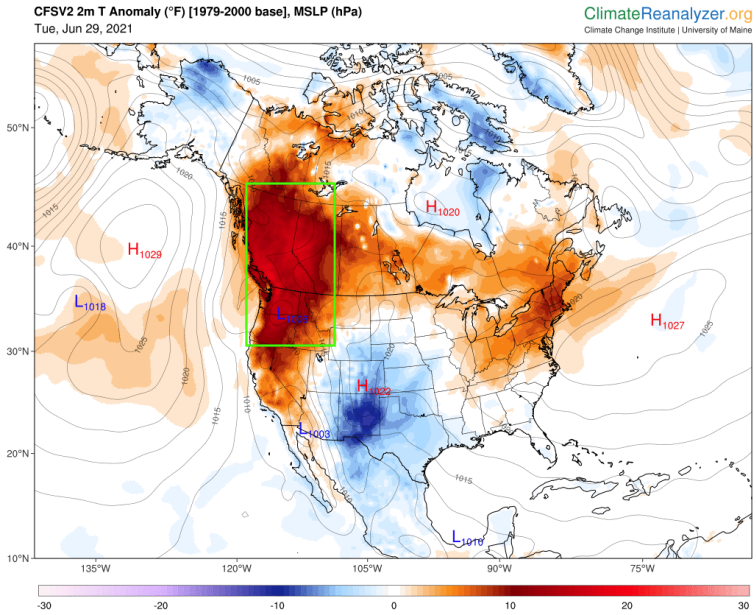

Figure 13. Air temperature (in °C) at 2 meters above sea surface over the North American area. Data map provided by the Climate Change Institute, University of Maine (https://climatereanalyzer.org).

Figure 14 shows the DMSP variation of electron density δNe during daytime (panel a) and during nighttime (panel b) respectively. Meanwhile, panel (c) shows data map of the air temperature at 2m over a 5-day period during 26-30 June 2021 obtained from NOAA (https://psl.noaa.gov/cgi-bin/data/narr/plotday.pl). All of these three plots cover the same geographic sector and are shown in the same scale. The area affected by the heat wave event, which we are interested in, is highlighted by a rectangular frame. It is clear from the data map that the temperature is higher below latitude 38°. Based on the plots of dayside δNe (panel a) and temperature *T* (panel c), it is quite apparent that δNe is proportional to *T*. However, during the nighttime the observed pattern shows the opposite behavior, where there was little or no wave fluctuations.

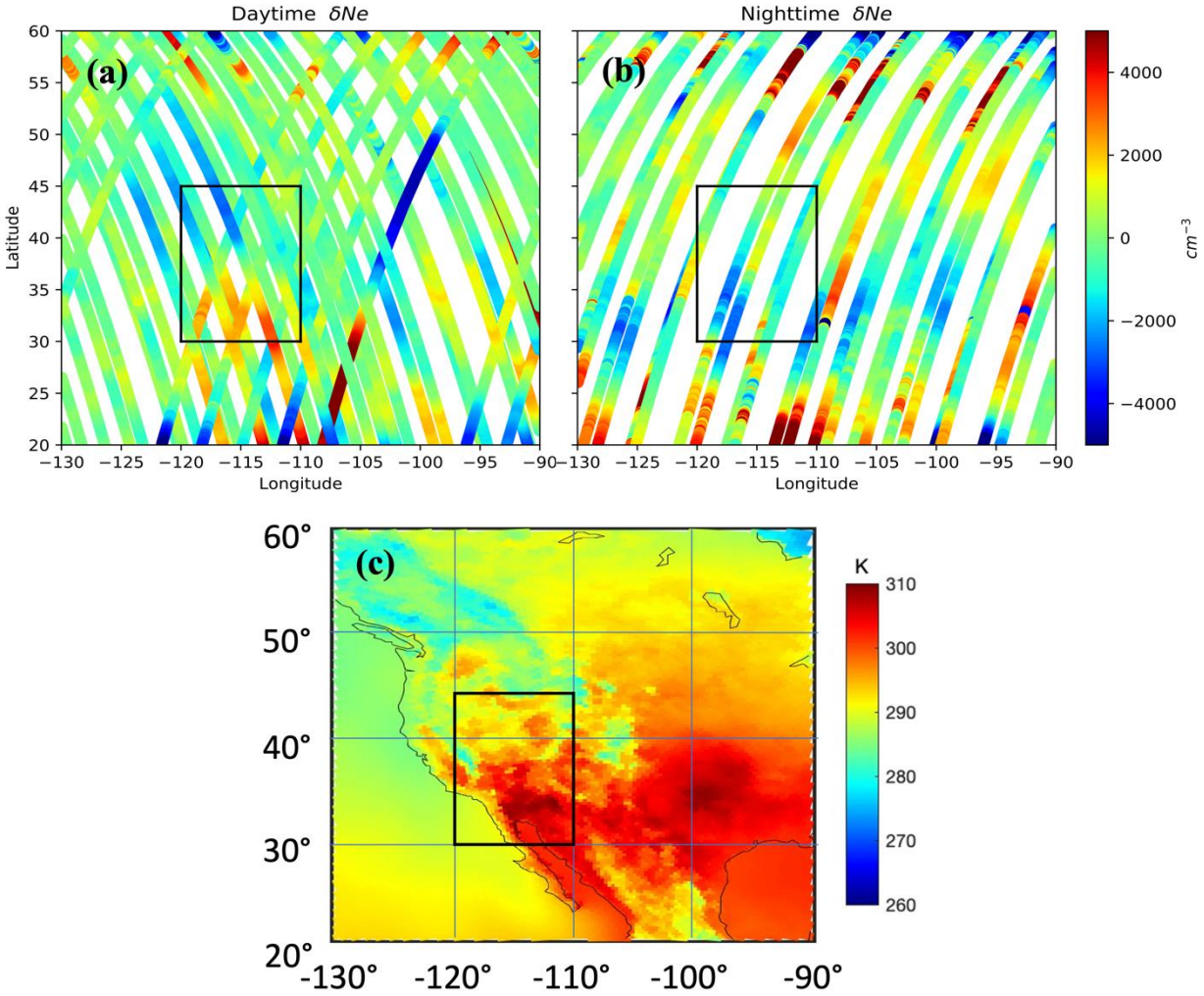

Figure 14. (a, b) Plots showing the variation of electron density δNe from DMSP observations over North America during the daytime and nighttime. (c) Data map showing NOAA data + model assimilation of 2m air temperature in the same area.

This initial DMSP data analysis of the summer 2021 heat wave event over North America seems to corroborate the scenario of increased level of ionospheric fluctuations during a severe heat wave event. More analysis will be needed for a more in-depth look of this heat wave impact on

the ionospheric fluctuations, including a cross-examination against regional GPS TEC data and weather/climate data . There are some interesting implications from this geophysical scenario, considering that more frequent and more severe heat wave events are anticipated as a result of climate change and global warming. We may be witnessing ionospheric space weather manifestations of climate change effects.

II. Impacts

The processing of DMSP data thus far has continued to make the data products available to the wider scientific community through the Madrigal database. Augmented by observations from other missions and numerous ground-based sensors, the data products serve as vital element for us to study notable ionospheric and space weather phenomena.

In the investigation of ionospheric disturbances associated with the 4 August 2020 Port Beirut explosion event, the DMSP data products played an important role in demonstrating that the disturbances were able to propagate over longer distances than previously known. A couple of prior studies about this notable man-made accident had detected disturbances in the near-field (within 500 km radius of the explosion site) using GNSS TEC observation data. No signs of these disturbances had been recognized at farther distances by the GNSS TEC observations alone. The DMSP observation data during this event, however, allowed us to show signatures of these ionospheric disturbances at significantly more distant locations, roughly 2000-3000 km away from the explosion site.

In the investigation of the Tonga volcano event, we have highlighted several key aspects of the accompanying ionospheric phenomena. One of these unique aspects is the azimuthal asymmetry of the ionospheric disturbances in the near-field, closely mimicking the shape of the tsunami wavefront around the Tonga region. Previously, much focus had been on the global reach of the disturbances from Tonga, which was largely isotropic with speed of Lamb waves. The other unique aspect was the impact these ionospheric disturbances had on GPS PPP performance in a rather unexpected way. It might have been anticipated a priori that the GPS PPP accuracy would be the one affected. We found, however, that it was not the case. Instead, it was the GPS PPP convergence times that were affected.

In the analysis of ionospheric irregularities during the summer 2021 heat wave event, we have discovered that the steady increase in the intensity of summer heat waves over the recent years may have extended consequences on our geospace environment. We may be witnessing a form of space weather manifestations of climate change effects that slowly become more pronounced.

Finally, when performing empirical tests for the concept of Shannon information content for characterizing perturbed ionospheric TEC configurations, we were able to involve a student (Bryce Kim) who participated in the 2022 Research Science Institute (RSI) program. Bryce also had the opportunity to present some results from his data analysis during the AGU Fall Meeting 2022 (https://agu.confex.com/agu/fm22/prelim.cgi/Paper/1062793). This has proven to be a fruitful educational experience through research activities for student.

References

Duncombe, J. (2022), The surprising reach of Tonga's giant atmospheric waves, *Eos*, 103, https://doi.org/10.1029/2022EO220050. Published on 21 January 2022.

Fountain, H. (2022), Here's What Scientists Know About the Tonga Volcano Eruption, *The New York Times*, Published 19 Jan 2022, Updated 21 Jan 2022, https://www.nytimes.com/2022/01/19/climate/scientists-tonga-volcano-eruption-effects.html

Francis, E., C. Parker, and R. Pannett (2022), Underwater Pacific volcano sends tsunami waves to Tonga, cutting off contact with outer islands, *The Washington Post*, Published 15 Jan 2022 at 5:01 a.m. EST, Updated 16 Jan 2022 at 3:36 a.m. EST.

Guglielmi, G. (2020), Why Beirut's ammonium nitrate blast was so devastating, *Nature*, 10 August 2020, https://doi.org/10.1038/d41586-020-02361-x

Gusman, A. R., and J. Roger (2022), Hunga Tonga - Hunga Ha`apai volcano-induced sea level oscillations and tsunami simulations, *GNS Science webpage*, Accessed at https://doi.org/10.21420/DYKJ-RK41 on 27 May 2022.

Jonah, O. F., Vergados, P., Krishnamoorthy, S., and Komjathy, A. (2021), Investigating ionospheric perturbations following the 2020 Beirut explosion event, *Radio Science*, 56, e2021RS007302, https://doi.org/10.1029/2021RS007302

Kubota. T., T. Saito, and K. Nishida (2022), Global fast-traveling tsunamis driven by atmospheric Lamb waves on the 2022 Tonga eruption, *Science*, https://doi.org/10.1126/science.abo4364

Kundu, B., Senapati, B., Matsushita, A. *et al.* Atmospheric wave energy of the 2020 August 4 explosion in Beirut, Lebanon, from ionospheric disturbances. *Sci Rep* **11,** 2793 (2021). https://doi.org/10.1038/s41598-021-82355-5

Nidumolu, J., R. Jose and C.-R. Kim (2022), Tonga volcano eruption triggers tsunami warnings in Japan, Pacific islands, *Reuters*, 15 January 2022, 23:59 PM EST, https://www.reuters.com/business/environment/tonga-volcano-generates-tsunami-us-tsunami-monitor-said-2022-01-15

Pilger, C., Gaebler, P., Hupe, P. et al. Yield estimation of the 2020 Beirut explosion using open access waveform and remote sensing data. *Sci Rep* **11**, 14144 (2021). https://doi.org/10.1038/s41598-021-93690-y

Sidder, A. (2022), Modeling atmospheric waves from Hunga Tonga–Hunga Haʻapai, *Eos*, 103, https://doi.org/10.1029/2022EO220240. Published on 12 May 2022.

United States Geological Survey (2022), M 5.8 Volcanic Eruption - 68 km NNW of Nuku`alofa, Tonga, *USGS Earthquake Hazards Program*,

https://earthquake.usgs.gov/earthquakes/eventpage/pt22015050/executive

Yuen, D. A., M. A. Scruggs, F. J. Spera, Y. Zheng, H. Hu, S. R. McNutt, G. Thompson, K. Mandli, B. R. Keller, S. S. Wei, Z. Peng, Z. Zhou, F. Mulargia, Y. Tanioka (2022), Under the surface: Pressure-induced planetary-scale waves, volcanic lightning, and gaseous clouds caused by the submarine eruption of Hunga Tonga-Hunga Ha`apai volcano, *Earthquake Research Advances*, 100134, https://doi.org/10.1016/j.eqrea.2022.100134.